1 Flight details

Aerosol forecast maps indicate the spatial sampling of the aerosol plumes for 31 August, 4 September, 6 September, 24 September, 25 September, of 2016, and 31 August, 2017, with the corresponding OA data and model-estimated age displayed on individual altitude-latitude flight track projections for each flight (Figs. S1-S2). A WRF-AAM-derived age example is shown for 24 September 2016 in Fig. S3, at 3 km altitude, in which tracers tagged to CO are released daily from 0-1 day to 7-8 days. Table S1 lists all of the ORACLES-2016 flights and includes comments on their flight pattern, the number of seconds with OA>20 μg m^{-3} if they were selected for analysis, and otherwise comments on why they were not selected for analysis. Table S2 provides the flight dates, location, time span and altitude of the level legs providing data.

2 Sampling Inlet

A high-resolution aerosol mass spectrometer, nephelometers, absorption and soot photometers, and CO/CO_2 analyzer were all situated behind a Solid Diffuser Inlet (SDI), with the nephelometers located closest to the inlet and the Aerosol Mass Spectrometer (AMS) and Single Particle Soot Photometer (SP2) located approximately 8m behind the inlet. The SDI brings ambient aerosol into the aircraft and can efficiently transmit aerosol particles smaller than 4μm in dry diameter (McNaughton et al., 2007). The SDI and ground-sampled submicron scattering data agreed to within 16% during the DC-8 Inlet Characterization Experiment (McNaughton et al., 2007). This establishes the particle loss to the inlet structure, instrument and tubing layout during the ORACLES campaign. Additionally, the sample flow through the inlet was measured and adjusted to ensure the air velocity equaled the flight speed to within 5%. This isokinetic sampling minimizes size-dependent sampling biases (Huebert et al., 1990). Although the inlet was maintained at isokinetic flow, the instruments required a constant flow. An online particle loss calculator (Aerocalc, created by Paul Baron, http://www.tsi.com/uploadedFiles/Product_Information/Literature/Software/Aerocalc2001.xls) selected tubing material, length, and diameter to minimize particle loss between the SDI and aircraft instruments. The inlet was anodized aluminum, with the flow split into tubes of stainless steel. All lines to the mass spectrometer relied on ½" stainless steel (outer diameter) and ¼" (outer diameter) copper tubing, to reduce the possible presence of extraneous organic compounds. The conductive tubing also minimizes electrophoretic losses. Tubing to the scattering, sizing and counting instruments consisted of graphite-impregnated silicone tubing, with condensation of any released organic compounds upon particles within the air stream unlikely to affect the particle size over the short distance. Due to differences in flow rates and paths, additional losses may affect some instruments more than others. Figures S7-S8 show the plumbing diagram of the aerosol instruments for each year. Calculated losses were negligible, if inherently optimistic and unable to account for all features of the hardware and instruments.

3 Wall losses

The $\sim$8 m distance from the SDI increases the potential for aerosol to deposit upon the tubing wall prior to reaching the AMS. Submicron aerosol is assumed to scatter 5 M m^{-1} at a wavelength of 500 nm per μg m^{-3} of aerosol mass (Reid et al., 1998; Haywood et al., 2003), termed by them as a mass scattering efficiency. Their result is used to assess if submicron aerosol was lost to wall deposition before reaching the AMS during the ORACLES campaign. The aerosol scattering was measured directly behind the inlet (TSI 3563, 550 nm wavelength) and divided by the total aerosol mass ascertained by the AMS. If the mass becomes depleted by wall losses, the mass scattering efficiency becomes increased. This ratio was evaluated at three different locations/altitudes, resulting in an average scattering by submicron aerosol was 5.92 M m^{-1} per μg m^{-3}. This is close to the expected value of 5, given that the uncertainty in the total aerosol mass concentration is almost 40%. This result constrains the wall losses to within 20% for the entire campaign, though with a wide error margin.

4 Aerosol sizing

The LDMA is heavily modified from a TSI 3071A electrostatic classifier. The flow control, neutralizer and high voltage systems have all been replaced, with only the original DMA column remaining (it is similar to the more recent TSI 3081 DMA). The initial system was modified to scan the voltage. This makes the original system similar to a Scanning Mobility Particle Sizer (SMPS) but the original nomenclature has been maintained here. The UHSAS optical spectrometer measures particles between 60-1000 nm at a higher one-second time resolution. An infrared laser illuminates particles, with the scattered light collected on two pairs of optical detectors. The particle sizes are then divided into 100 user-specific size bins. The UHSAS undersizes almost 30% of black carbon containing particles during ORACLES (Howell et al., 2021), because of incorrect refractive indices assumptions (n_r=1.588, n_i=0). A correction for the undersizing is evaluated in Fig. S5. Fig. S6 assesses the thermal DMA size distributions for 31 August 2017, 12:14:54, at STP, 150°C and 300°C, done to evaluate the aerosol volatility. As shown, the TDMA size distributions remain consistent regardless of temperature, providing a further indication of low aerosol volatility.

5 Aerosol Mass Spectrometer

The AMS sampled the chemical composition of non-refractory aerosols with vacuum aerodynamic diameters between approximately 70 nm to 700 nm at a rate of 1.38 cm^3 s^{-1}. An aerodynamic lens selects and focuses particles at a constant 600 hPa pressure onto a 650°C heated surface. The non-refractory particles are then evaporated off the heated surface and ionized through electron impaction at 70 eV; the ions are carried forward and analyzed further, with some particles, such as soot, some organics, dust, and some salts remaining unvaporized (and unanalyzed). A 'V-mode' operation provided a higher time resolution for the same signal-to-noise, with only a modest loss in the mass resolution (see DeCarlo et al., 2006, for more description). The AMS chopper alternately open and closed every two seconds, to allow aerosol into the AMS and to then analyze it, with an additional second separating each duty cycle.

The bulk mass (not size-resolved) chemical species measurements are primarily processed using the SeQUential Igor data RetRiEval (SQUIRREL, v.1.57l Allan et al., 2003, 2004) data analysis package, with the Peak Integration by Key Analysis (PIKA) program (v.1.16; DeCarlo et al., 2006) resolving the O:C, H:C and OA:OC ratios. Further considerations for the ORACLES AMS-derived aerosol mass concentration data accuracies include the instrument detection threshold, calibrations, and discrimination for organic versus inorganic nitrate. These are considered in that order. Many of the data quality assurance procedures follow those within Shank et al. (2012).

The aircraft-based background values are determined from the noise levels measured at 15,000 ft during a 10-minute time period on the 4 September, 2016 flight. This established detection limits of 0.15 μg m^{-3} for organics, 0.04 μg m^{-3} for nitrate, 0.03μg m^{-3} for sulfate, and 0.01μg m^{-3} for ammonium. Chloride mass, which nominally contributed $< 1\%$ of the total free-tropospheric aerosol mass, was excluded as its ionization signature varies strongly with composition and exact instrument configuration. Detection limits typically improve during a flight as the background material becomes effused. The AMS was heated pre-flight during the 2016 campaign to eliminate material built up in between flights. During the 2017 campaign, an initial high-altitude remote sensing leg provided time to drive off extraneous material before beginning the in-situ sampling.

The AMS was calibrated twice during the 2016 campaign (at the beginning and end), and after every 2-3 flights during the 2017 campaign for a total 8 calibrations, using ammonium nitrate particles. An ammonium nitrate solution is sent through an atomizer to produce desiccated submicron aerosol that is then sent to the AMS. A long differential mobility analyzer (LDMA) (heavily modified from a TSI 3071A electrostatic classifier) selects for 300 nm diameter particles, and a condensation particle counter (TSI 3010) measures the aerosol number concentration. The ammonium nitrate aerosol is diluted by a factor of four in the atomizer to create a calibration curve. The ionization efficiency (IE) of nitrate is thereafter calculated from the aerosol mass and number concentrations. The ionization efficiency estimates the number of ions from a known amount of mass entering the AMS using the ion signals at *m/z* peak 30 (NO^+) and 46 (NO_2^+). The nitrate IE values centered on 1.31e-7, with a nominal 10% uncertainty assigned to it following Bahreini et al. (2009), slightly higher than the 1e-7 value within Alfarra et al. (2004). The ionization efficiencies for ammonium, sulfate and organics relative to those for nitrate are thereafter determined within SQUIRREL as: 4 for NH_4; 1.1 for measured nitrate relative to the calibration value; 1.2 for SO_4; and 1.4 for organics.

A time- and composition-dependent collection efficiency (CE) corrects for the incomplete vaporization of mixed phase particles (Middlebrook et al., 2012), as liquid aerosol is less likely to bounce off the heater and more likely to escape detection than is neutralized aerosol (Huffman et al., 2005; Drewnick et al., 2005). Liquid aerosol is primarily acidic, and the acidity of the free-tropospheric aerosol is assessed by comparing the molar ratio of NH_4 to NO_3+2SO_4 (Fig. S9). This is a simplification of the $NH_{4,measured}/NH_{4,predicted}$ relationship put forth in Zhang et al. (2007), with the contribution of chloride neglected because it is small. $NH_{4,predicted}$ is the amount of ammonium required to neutralize the inorganic anions observed by the AMS. The applied collection efficiency, $CE = max(0.5, 1 - \frac{NH_4}{2SO_4})$, also neglects the small nitrate contribution, and establishes 0.5 as the lower limit, consistent with most field campaigns (Middlebrook et al., 2012). The ratio of the measured ammonium to the molar sum of nitrate and 2*sulphate is mostly below 1, but rarely below 0.75 (Fig. S9), typically establishing a CE of 0.5. The mildly acidic aerosol suggests mild suppression of inorganic acid formation. Wu et al. (2020) report nitrate aerosol that is fully neutralized based on independent AMS measurements from August-September 2017 further west of the ORACLES sampling, above Ascension Island (8°S, 14.5°W). This indicates further loss of the organic nitrate may be occurring between the ORACLES and Ascension locations. The CE values for the other species are set to 0.5; Middlebrook et al. (2012) do not find any dependence of the CE on the mass fraction of organics.

The overall uncertainty to the reported aerosol mass concentrations is likely dominated by the uncertainty in CE, with additional uncertainty in the organic RIE. Fig. S4a shows the OA:BC mass ratios as a function of model age for OA > 3 μg m^{-3} (blue) and OA >20 μg m^{-3} (black), while Fig. S4b shows percentiles of the OA:BC mass ratio composited by aerosol mass bins. Fig. S10-S11 shows the nondimensional BC:ΔCO as a function of *f44* for each flight with sufficient OA $>$ 20 and 10 g m^{-3}, and Figs. S12-S13 shows the corresponding OA:BC values.

6 Gas measurements

Carbon monoxide was measured with an aircraft modified gas-phase CO/CO_2/H_2O Analyzer from Los Gatos Research, operated and analyzed by NASA Ames (Jim Podolske). The analyzer uses a patented Integrated Cavity Output Spectroscopy (ICOS) technology to make stable cavity-enhanced absorption measurements of CO, CO_2, and H_2O in the infrared spectral region. The instrument reports CO mixing ratio (mole fraction) at a 1-Hz rate based on measured absorption, gas temperature, and pressure using Beer's Law (Zellweger et al., 2012). The measurement precision is 0.5 ppbv over 10 seconds.

7 Background on the optical measurements

The nephelometer measurements occurred at 40-50% relative humidity. Ambient RH measurements ranged up to 80%, with higher RH data samples excluded by construction. The humidity impact on the nephelometer measurements was examined using two other single-wavelength (550 nm) nephelometers (Radiance Research, M903) measured at two different relative humidities, one at 80% and the other at below 40% RH (Howell et al., 2006). The impact on light scattering, estimated from the ratio of the ambient to dry RH measurements, is estimated to be less than 1.2 for 90% of the time (Shinozuka et al., 2020). The 20% increase in scattering by the ambient RH is an upper bound, as the ambient RH is typically <80%. The nephelometer filter-based measurements are corrected according to Anderson and Ogren (1998).

The PSAP measurements measured at a lower $\sim$ 20% RH, brought about by heating the PSAP optical block to approximately 50°C. The scattering absorption coefficients (σ_as) are an average of two PSAP measurements in 2016, with only one PSAP functioning in 2017. Corrections to the absorption coefficients are based on the wavelength-averaged (as opposed to wavelength-length-specific) values from Virkkula (2010). The use of the average wavelength-corrected values reduces a potential high bias from multiple scattering at the shortest wavelength (Pistone et al., 2019), and reduces spurious effects from filter changes (Zuidema et al., 2018). Compared to Pistone et al. (2019), a stricter aerosol threshold is applied (OA>20 μg m^{-3} rather than scattering at 530nm > 10 Mm^{-1}) and no arithmetic weighting by extinction is done. SSA values at 530 nm are at standard temperature and pressure. Aerosol absorption can also increase because of humidification (see discussion in Pistone et al. (2019)), introducing a compensating effect on the SSA, but this is likely smaller.

Two nephelometers (TSI 3565), located near the aerosol inlet, were also used to assess the contribution of submicron aerosol to the total aerosol scattering. One nephelometer measured only the submicron scattering, while the second nephelometer

measured both total and submicron scattering. The measured total to submicron scattering ratio was 1.02, confirming that almost all of the free-tropospheric scattering is by submicron aerosol.

Author contributions. The present work was conceived by PZ, AD, SH and PS. SF contributed to the HiGEAR data analysis, AS provided the BC datasets and PS the WRF-AAM model age estimates. Portions of this work first appeared in the M.S. thesis of A.D at U. of Hawaii. PZ led the writing and AD provided most of the figures, with all authors contributing to the final writing.

Competing interests. Paquita Zuidema is a guest editor for the ACP Special Issue: "ACP special issue: New observations and related modelling studies of the aerosol–cloud–climate system in the Southeast Atlantic and southern Africa regions" The other authors declare no competing interests.

Acknowledgements. ORACLES is a NASA Earth Venture Suborbital-2 investigation, funded by the US National Aeronautics and Space Administration (NASA)'s Earth Science Division and managed through the Earth System Science Pathfinder Program Office (grant no. NNH13ZDA001N-EVS2). This work was further supported by the US Department of Energy (DOE: grant DE-SC0018272 to P.Z. and P.S. and DE-SC0021250 to P.Z.).

References

Alfarra, M. R., Coe, H., Allan, J. D., Bower, K. N., Boudries, H., Canagaratna, M. R., Jimenez, J. L., Jayne, J. T., Garforth, A. A., Li, S.-M., and Worsnop, D. R.: Characterization of urban and rural organic particulate in the Lower Fraser Valley using two Aerodyne Aerosol Mass Spectrometers, Atmos. Env., 38, 5745–5758, https://doi.org/10.1016/j.atmosenv.2004.01.054, 2004.

Allan, J. D., Jimenez, J. L., Williams, P. I., Alfarra, M. R., Bower, K., Jayne, J., Coe, H., and Worsnop, D.: Quantitative sampling using an Aerodyne aerosol mass spectrometer: 1. Techniques of data interpretation and error analysis, J. Geophys. Res., 108, 4090–, https://doi.org/10.1029/2002JD002358, 2003.

Allan, J. D., Delia, A. E., Coe, H., Bower, K. N., Alfarra, M. R., Jimenez, J. L., Middlebrook, A. M., Drewnick, F., Onasch, T., and et al., M. C.: A generalised method for the extraction of chemically resolved mass spectra from Aerodyne aerosol mass spectrometer data, J. Aerosol Sci., 35, 909–922, 2004.

Anderson, T. L. and Ogren, J. A.: Determining Aerosol Radiative Properties Using the TSI 3563 Integrating Nephelometer, Aer. Sci. Tech., 29, 57–69, https://doi.org/10.1080/02786829808965551, 1998.

Bahreini, R., Ervens, B., Middlebrook, A. M., Warneke, C., de Gouw, J. A., DeCarlo, P. F., and et al., J. L. J.: Organic aerosol formation in urban and industrial plumes near Houston and Dallas, Texas, J. Geophys. Res., 114, https://doi.org/10.1029/2008jd011493, 2009.

DeCarlo, P. F., Kimmel, J. R., Trimborn, A., Northway, M. J., Jayne, J. T., and et al., A. C. A.: Field-deployable, high-resolution, time-of-flight aerosol mass spectrometer, Anal. Chem., 78, 8281–8289, https://doi.org/10.1021/ac061249n, 2006.

Drewnick, F., Hings, S. S., DeCarlo, P., Jayne, J. T., Gonin, M., Fuhrer, K., Weimer, S., and et al., J. L. J.: A New Time-of-Flight Aerosol Mass Spectrometer (TOF-AMS)—Instrument Description and First Field Deployment, Aer. Sci. Tech., 39, 637–658, https://doi.org/10.1080/02786820500182040, 2005.

Haywood, J. M., Osborne, S. R., Francis, P. N., Keil, A., Andreae, P. F. M. O., and Kaye, P. H.: The mean physical and optical properties of regional haze dominated by biomass burning aerosol measured from the C-130 aircraft during SAFARI 2000, J. Geophys. Res., 108, 8473–8481, https://doi.org/10.1029/2002JD002226, 2003.

Howell, S. G., Clarke, A. D., Shinozuka, Y., Kapustin, V., McNaughton, C. S., Huebert, B. J., Doherty, S. J., and Anderson, T. L.: Influence of relative humidity upon pollution and dust during ACE-Asia: Size distributions and implications for optical properties, J. Geophys. Res., 111, https://doi.org/10.1029/2004JD005759, 2006.

Howell, S. G., Freitag, S., Dobracki, A., Smirnow, N., and III, A. J. S.: Undersizing of aged African biomass burning aerosol by an ultra-high-sensitivity aerosol spectrometer, Atmos. Meas. Tech., 14, 7381–7404, https://doi.org/10.5194/amt-14-7381-2021, 2021.

Huebert, B. J., Lee, G., and Warren, W. L.: Airborne Aerosol Inlet Passing Efficiency Measurement, J. Geophys. Res., 95, 16 369–16 381, 1990.

Huffman, J. A., Jayne, J. T., Drewnick, F., Aiken, A. C., Onasch, T., Worsnop, D. R., and et al., J. L. J.: Design, Modeling, Optimization, and Experimental Tests of a Particle Beam Width Probe for the Aerodyne Aerosol Mass Spectrometer, Aer. Sci. Tech., 39, 1143–1163, https://doi.org/10.1080/02786820500423782, 2005.

McNaughton, C. S., Clarke, A. D., Howell, S. G., Pinkerton, M., Anderson, B., Thornhill, L., Hudgins, C., Winstead, E., Dibb, J. E., Scheuer, E., and Maring, H.: Results from the DC-8 Inlet Characterization Experiment (DICE): Airborne Versus Surface Sampling of Mineral Dust and Sea Salt Aerosols, Aer. Sci. Tech., 41, 136–159, https://doi.org/10.1080/02786820601118406, 2007.

Middlebrook, A. M., Bahreini, R., Jimenez, J. L., and Canagaratna, M. R.: Evaluation of Composition-Dependent Collection Efficiencies for the Aerodyne Aerosol Mass Spectrometer using Field Data, Aer. Sci. Techn., 46, 258–271, https://doi.org/10.1080/02786826.2011.620041, 2012.

Pistone, K., Redemann, J., Doherty, S., Zuidema, P., Burton, S., Cairns, B., Cochrane, S., Ferrare, R., Flynn, C., Freitag, S., Howell, S., Kacenelenbogen, M., LeBlanc, S., Liu, X., Schmidt, K. S., Sedlacek III, A. J., Segal-Rosenhaimer, M., Shinozuka, Y., Stamnes, S., van Diedenhoven, B., Van Harten, G., and Xu, F.: Intercomparison of biomass burning aerosol optical properties from in-situ and remote-sensing instruments in ORACLES-2016, Atmos. Chem. Phys., 19, 9181–9208, https://doi.org/10.5194/acp-19-9181-2019, 2019.

Reid, J. S., Hobbs, P. V., Ferek, R. J., Blake, D. R., Martins, J. V., and Liousse, M. R. D. C.: Physical, chemical, and optical properties of regional hazes dominated by smoke in Brazil, J. Geophys. Res., 103, 32 059–32 080, https://doi.org/10.1029/98jd00458, 1998.

Shank, L. M., Howell, S., Clarke, A. D., Freitag, S., Brekhovskikh, V., Kapustin, V., McNaughton, C., Campos, T., and Wood, R.: Organic matter and non-refractory aerosol over the remote Southeast Pacific: oceanic and combustion sources, Atmos. Chem. Phys., 12, 557–576, https://doi.org/10.5194/acp-12-557-2012, 2012.

Shinozuka, Y., Saide, P. E., Ferrada, G. A., Burton, S. P., Ferrare, R., Doherty, S. J., Gordon, H., Longo, K., Mallet, M., Feng, Y., Wang, Q., Cheng, Y., Dobracki, A., Freitag, S., Howell, S. G., LeBlanc, S., Flynn, C., Segal-Rosenhaimer, M., Pistone, K., Podolske, J. R., Stith, E. J., Bennett, J. R., Carmichael, G. R., da Silva, A., Govindaraju, R., Leung, R., Zhang, Y., Pfister, L., Ryoo, J.-M., Redemann, J., Wood, R., and Zuidema, P.: Modeling the smoky troposphere of the southeast Atlantic: a comparison to ORACLES airborne observations from September of 2016, Atmos. Chem. Phys., 20, 11,491–11,526, https://doi.org/10.5194/acp-20-11491-2020, 2020.

Virkkula, A.: Correction of the Calibration of the 3-wavelength Particle Soot Absorption Photometer (3 PSAP), Aerosol Sci. Tech., 44, 706–712, 2010.

Wu, H., Taylor, J. W., Szpek, K., Langridge, J. M., Williams, P. I., Flynn, M., Allan, J. D., Abel, S. J., Pitt, J., Cotterell, M. I., Fox, C., Davies, N. W., Haywood, J., and Coe, H.: Vertical variability of the properties of highly aged biomass burning aerosol transported over the southeast Atlantic during CLARIFY-2017, Atmos. Chem. Phys., 20, 12 697–12 719, https://doi.org/10.5194/acp-20-12697-2020, 2020.

Zellweger, C., Steinbacher, M., and Buchmann, B.: Evaluation of new laser spectrometer techniques for in-situ carbon monoxide measurements, Atmos. Meas. Tech., 5, 2555–2567, 2012.

Zhang, Q., Jimenez, J. L., Worsnop, D. R., and Canagaranta, M.: A Case Study of Urban Particle Acidity and Its Influence on Secondary Organic Aerosol, Environ Sci. Technol., 41, 3213–3219, https://doi.org/10.1021/es061812j, 2007.

Zuidema, P., Sedlacek III, A. J., Flynn, C., Springston, S., Delgadillo, R., Zhang, J., Aiken, A. C., Koontz, A., and Muradyan, P.: The Ascension Island Boundary Layer in the Remote Southeast Atlantic is Often Smoky, Geophys. Res. Lett., 45, 4456–4465, https://doi.org/10.1002/2017gl076926, 2018.

Table S1. ORACLES flights occurring between August 31 and September 31. Examined flights in bold.

Date (M/DD/YYYY)	Flight label	Flight Description	sec. with OA>20 μg m^{-3} and BC, CO, SSA
8/27/2016	PRF00Y16	transit	probes off
8/30/2016	PRF01Y16	routine	aborted
8/31/2016	PRF02Y16	routine	**3,447**
9/02/2016	PRF03Y16	target	no OA>20, 6,341>10 μg m^{-3}
9/04/2016	PRF04Y16	routine	**1,760**
9/06/2016	PRF05Y16	target	**3,765**
9/08/2016	PRF06Y16	routine	aerosol age>10 days (too old)
9/10/2016	PRF07Y16	routine	aerosol age>10 days (too old)
9/12/2016	PRF08Y16	routine	38
9/14/2016	PRF09Y16	target	161
9/18/2016	PRF10Y16	target	no BC data
9/20/2016	PRF11Y16	target	no OA>20, 2,840>10 μg m^{-3}
9/24/2016	PRF12Y16	target	**4,072**
9/25/2016	PRF13Y16	routine	**2,732**
9/27/2016	PRF14Y16	transit	probes off
8/31/2017	PRF12Y17	target	**11,743**

Table S2. Level legs

Flight	Latitude °N	Longitude °E	Time (UTC)	Altitude (m)
08312016 (PRF02Y16)	-13.8 :-13.13	3.7:3.9	11:14-11:27	3830
09062016 (PRF05Y16)	-12.9:-12.2	9.2:9.5	11:40-11:50	2670
09062016 (PRF05Y16)	-15.9:-15.17	10.3:10.5	12:18-12:28	2250
09242016 (PRF12Y16)	-12.1:-11.0	11.0	12:08-12:21	4830
09252016 (PRF13Y16)	-9.8:-8.9	-0.344:-1.0	12:16-12:32	4500
08312017 (PRF12Y17)	-8.6:-7.5	-1.27:-0.88	11:43-11:57	3100
08312017 (PRF12Y17)	-7.5:-6.7	-1.58:-1.3	11:31-11:42	3035
08312017 (PRF12Y17)	-6.4:-5.6	-1.99:-1.65	11:15-11:30	2935
08312017 (PRF12Y17)	-5.29:-4.12	-1.64:- 2.01	10:52-11:11	2870
08312017 (PRF12Y17)	-8:-5.12	-1.09:-2.15	12:12-12:50	2970
08312017 (PRF12Y17)	-2.5:-0.5	-0.44:0.8	14:10-14:34	2880
08312017 (PRF12Y17)	-1.9:-1.23	-0.105:-0.404	1:55-14:05	2720
08312017 (PRF12Y17)	-2.4:-1.35	-0.70:-0.15	13:32-13:48	2570
08312017 (PRF12Y17)	-3.8:-1.27	-0.12:-1.49	10:12-10:49	2790

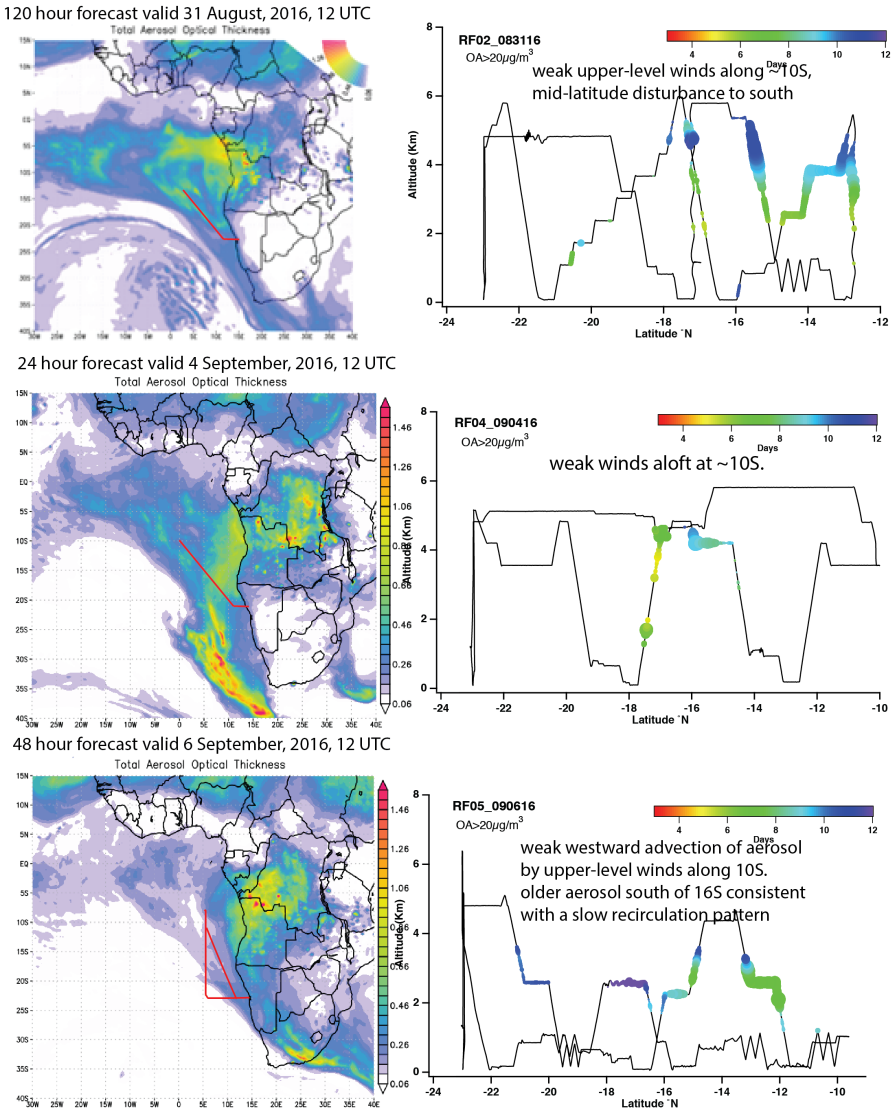

Figure S1. left) Global Modeling and Assimilation Office aerosol optical thickness forecasts for 31 August, 2016; 4 September, 2016; 6 September, 2016. Right) Altitude versus latitude cross-sections of the flights overlain with the colorized aerosol age, with the size of the marker providing a qualitative marker of aerosol mass.

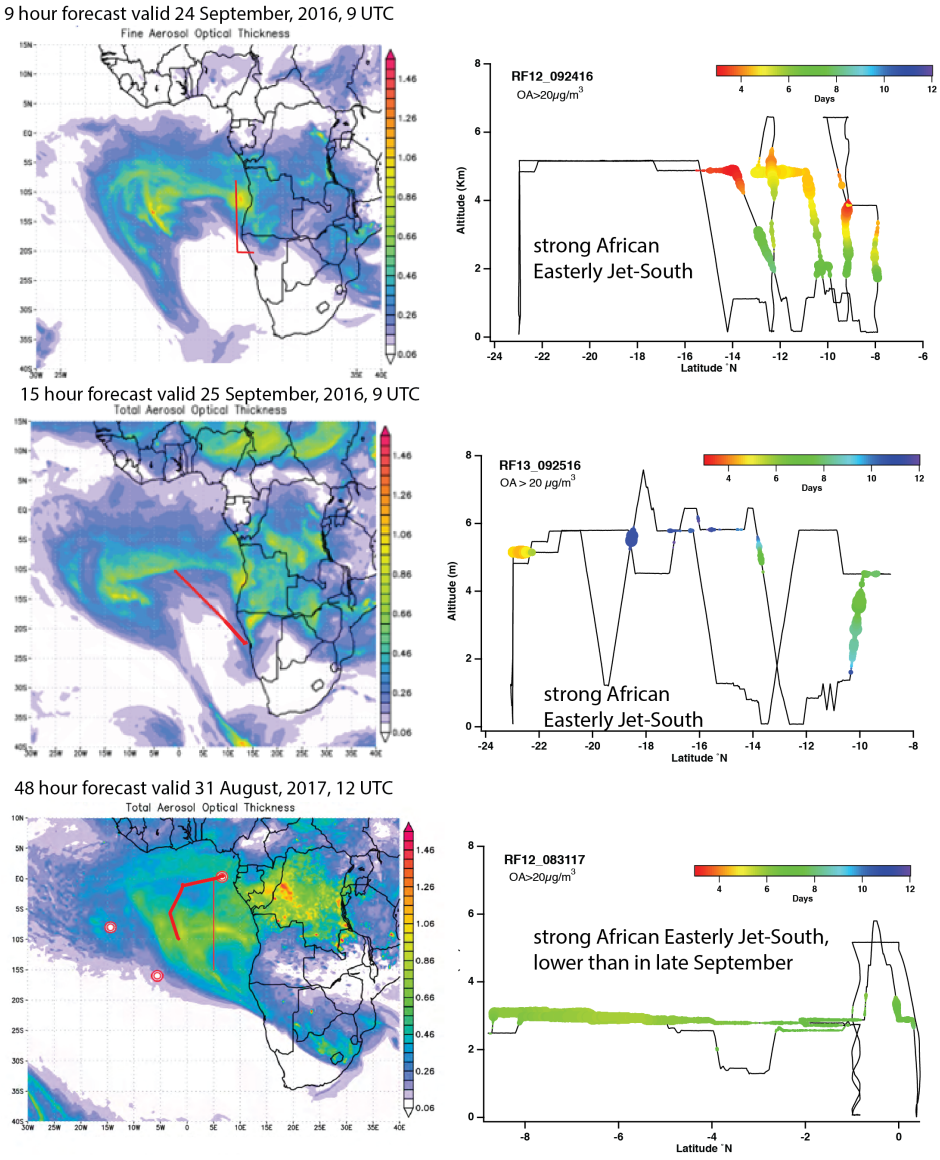

Figure S2. left) same as Fig. S1 but for 24 September, 2016; 25 September, 2016, and 31 August, 2017.

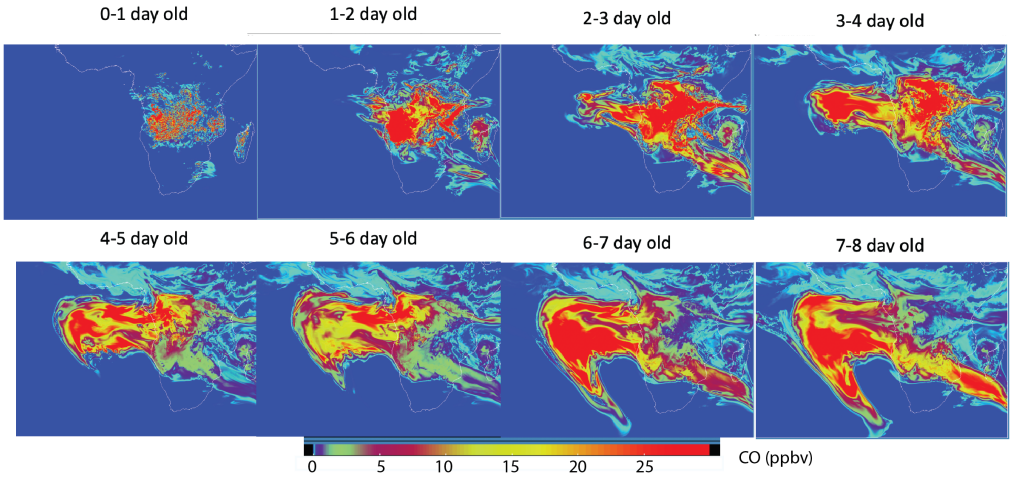

Figure S3. 24 September 2016 WRF-AAM CO-tracer from 0-1 up to 7-8 days since emission, at $\sim$ 3 km altitude. CO units in ppbv, with zero background CO.

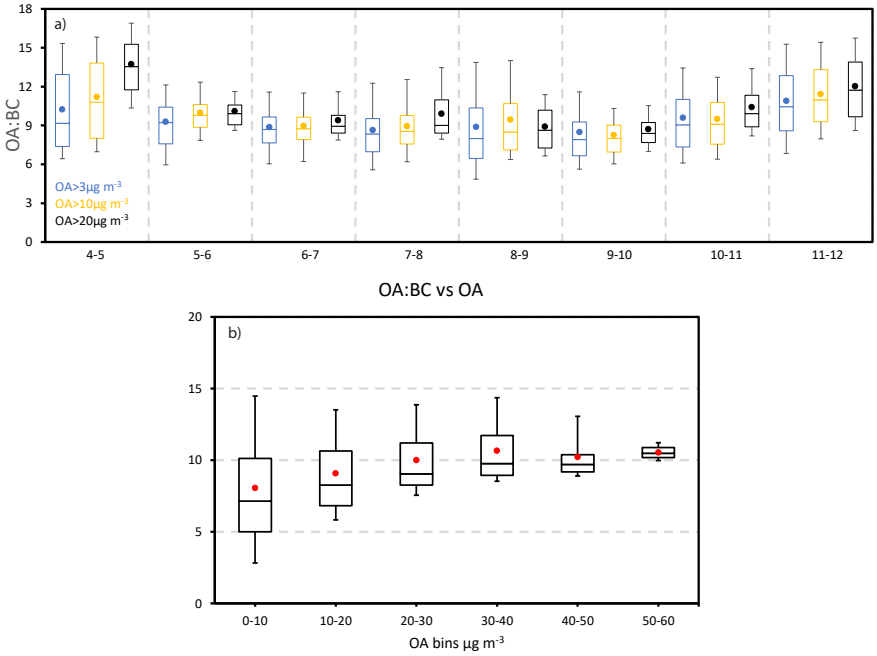

Figure S4. a) OA:BC mass ratio as a function of model age for OA > 3 μg m^{-3} (blue) and OA >20 μg m^{-3} (black). b) OA:BC mass ratio composited by aerosol mass bins, shown using 10, 25, 50, 75 and 90th percentiles, with means in red.

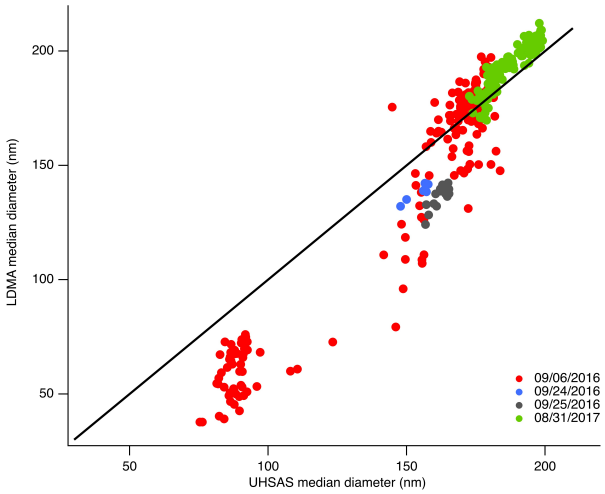

Figure S5. LDMA versus UHSAS median diameters for samples within the level-leg plumes (Table S2) with OA >20 μg m^{-3}, at one-minute time resolution.

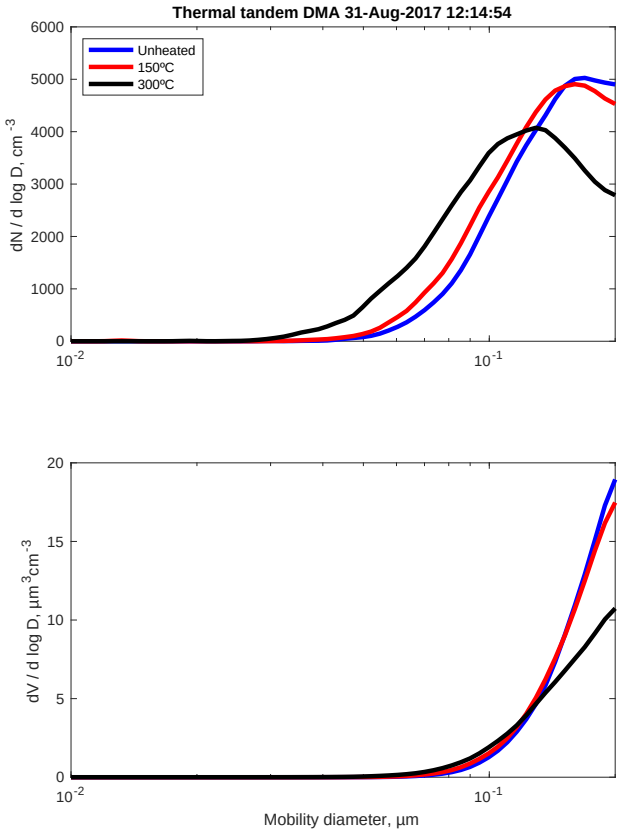

Figure S6. TDMA number (top) and volume (bottom) size distributions as a function of standard temperature and pressure (blue), heated to 150°C (red) and 300 °C (black), for 31 August 2017, 12:14:54.

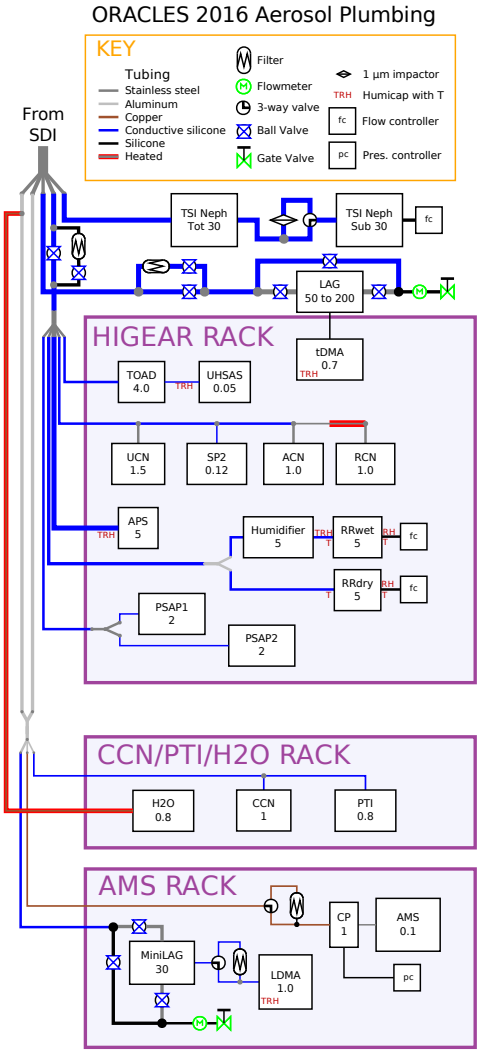

Figure S7. Layout of aerosol instrumentation relative to the inlet for the 2016 campaign. The numbers below the instrument acronyms represent flow rates in lpm. Note the lag and mini-lag include a small leak included to equalize the pressure between the two. The line widths are proportional to the nominal diameter of the tubing (outer for metal, inner for silicone). Exceptions are the AMS, SP2, and UHSAS, which have very low flow rates and such tiny inlet tubes that they wouldn't be visible. Acronyms, in alphabetical order: ACN=Ambient Condensation Nuclei (unheated TSI 3010); APS=aerodynamic particle sizer (TSI; LAG=Lagged Aerosol Chamber; CP=Constant Pressure inlet to the AMS. RCN=Refractory Condensation Nucleus Counter (TSI 3010, operated at 400°C); RR_{wet}=humidified Radiance Research nephelometer; RR_{dry}=Radiance Research nephelometer at 550 nm wavelength and low relative humidity; TOAD=thermo-optical aerosol discriminator; UCN=Ultrafine Condensation Nucleus Counter (TSI 3025, diameters > 2.5 μm). Other acronyms are described within the main text. Not all of these instruments were used for this analysis, and a particle cavity aerosol spectrometer probe (PCASP) operated by U of North Dakota is not shown here.

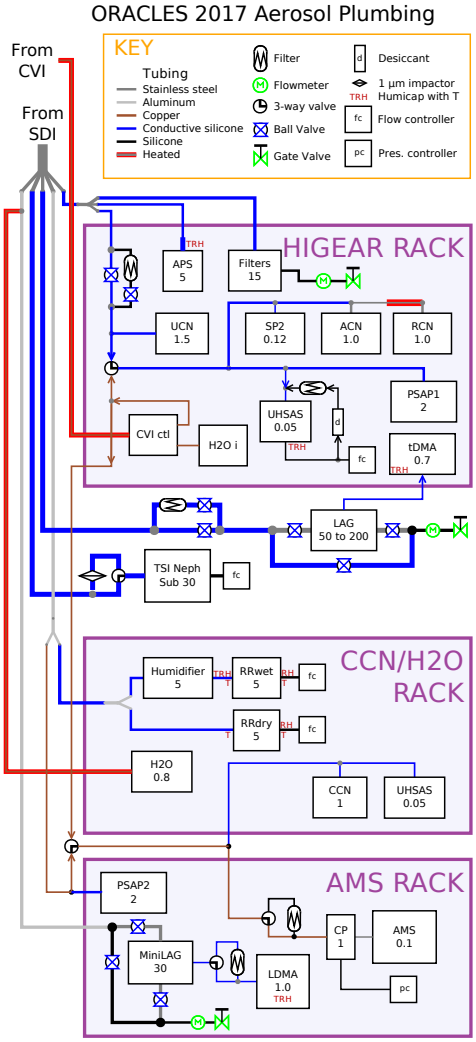

Figure S8. Layout of aerosol instrumentation relative to the inlet for the August 31, 2017 flight. Most flow is down and to the right, the addition of a counter-flow virtual impactor inlet (CVI) modified some flow direction to be up and to the left; flow direction arrows are included in critical spots to aid understanding. Other comments on the diagram Fig. S7 for 2016 also apply here.

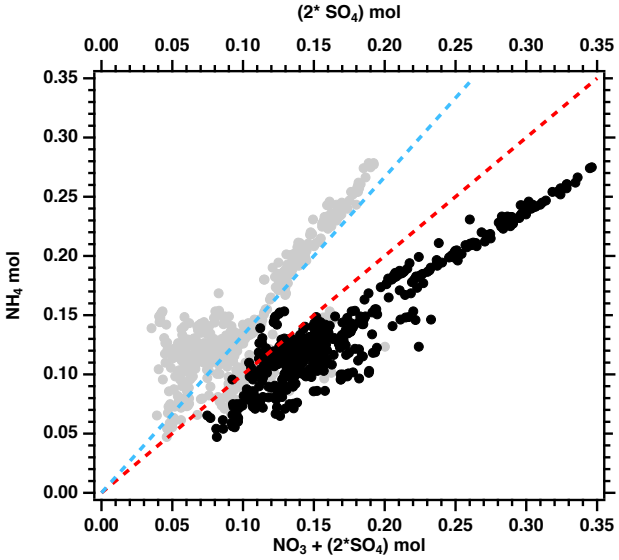

Figure S9. Measured ammonium in moles as a function of the molar sum of nitrate and 2*sulphate for one-minute measurements from all 6 flights (one-minute averages), constrained to the free troposphere. Dashed-red and dashed-blue lines indicate the 1:1 and 1:0.75 ratios respectively.

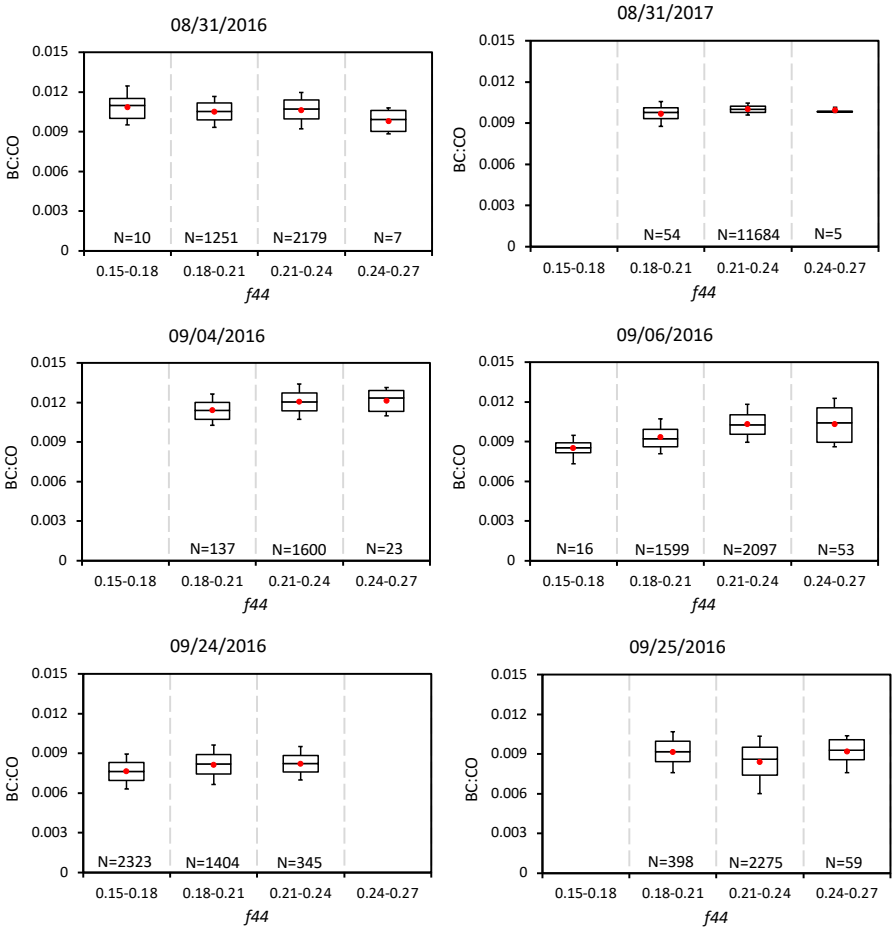

Figure S10. BC:ΔCO ratios (dimensionless) as a function of *f44* for the six flights. Whiskers represent the 10th and 90th percentiles, boxes illustrate the 75th and 25th percentiles with a line indicating the median and a red filled circle the mean. OA>20 μg m^{-3} only. The number of 1-second samples contributing to each *f44* bin of each flight is also indicated.

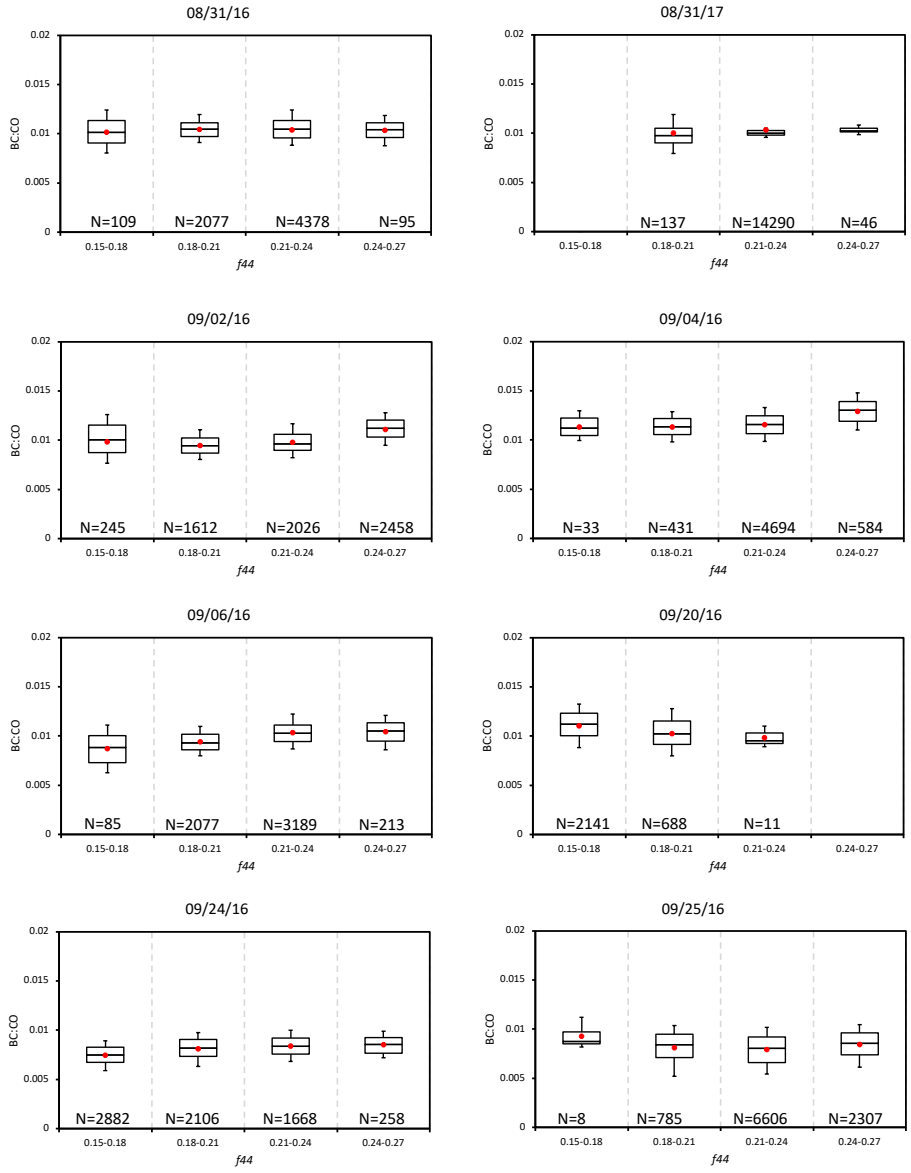

Figure S11. BC:ΔCO ratios (dimensionless) as a function of *f44* for the six flights. Whiskers represent the 10th and 90th percentiles, boxes illustrate the 75th and 25th percentiles with a line indicating the median and a red filled circle the mean. OA>10 μg m^{-3} only. The number of 1-second samples contributing to each *f44* bin of each flight is also indicated.

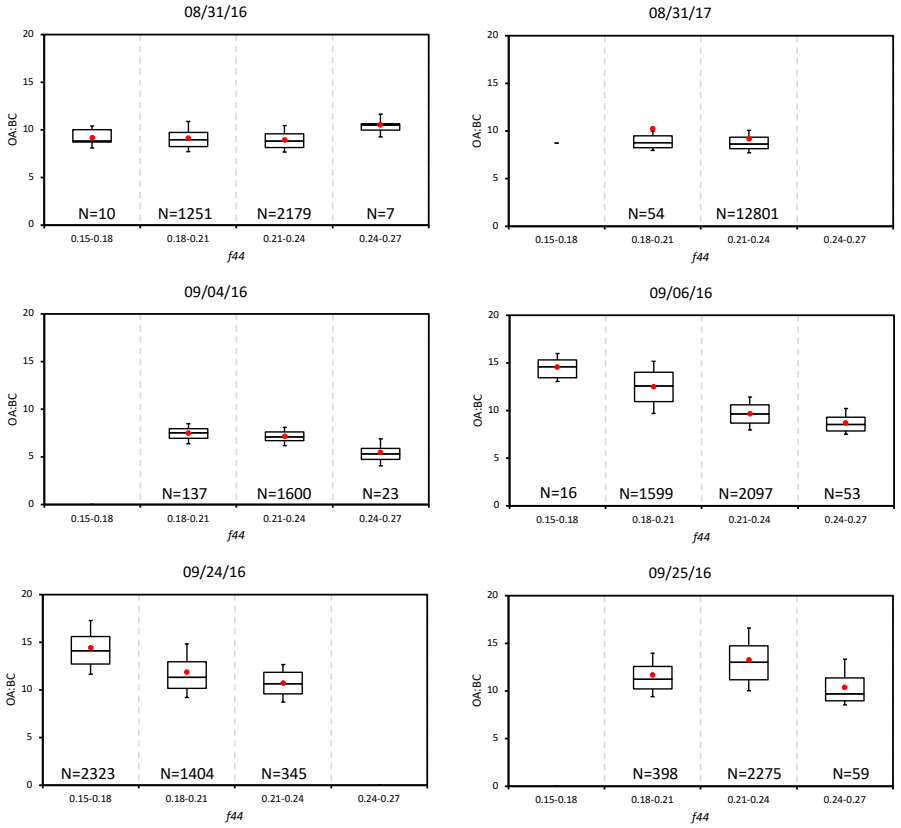

Figure S12. OA:BC mass ratios as a function of *f44* for the six flights. Whiskers represent the 10th and 90th percentiles, boxes illustrate the 75th and 25th percentiles with a line indicating the median and a red filled circle the mean. OA>20 μg m^{-3} only.

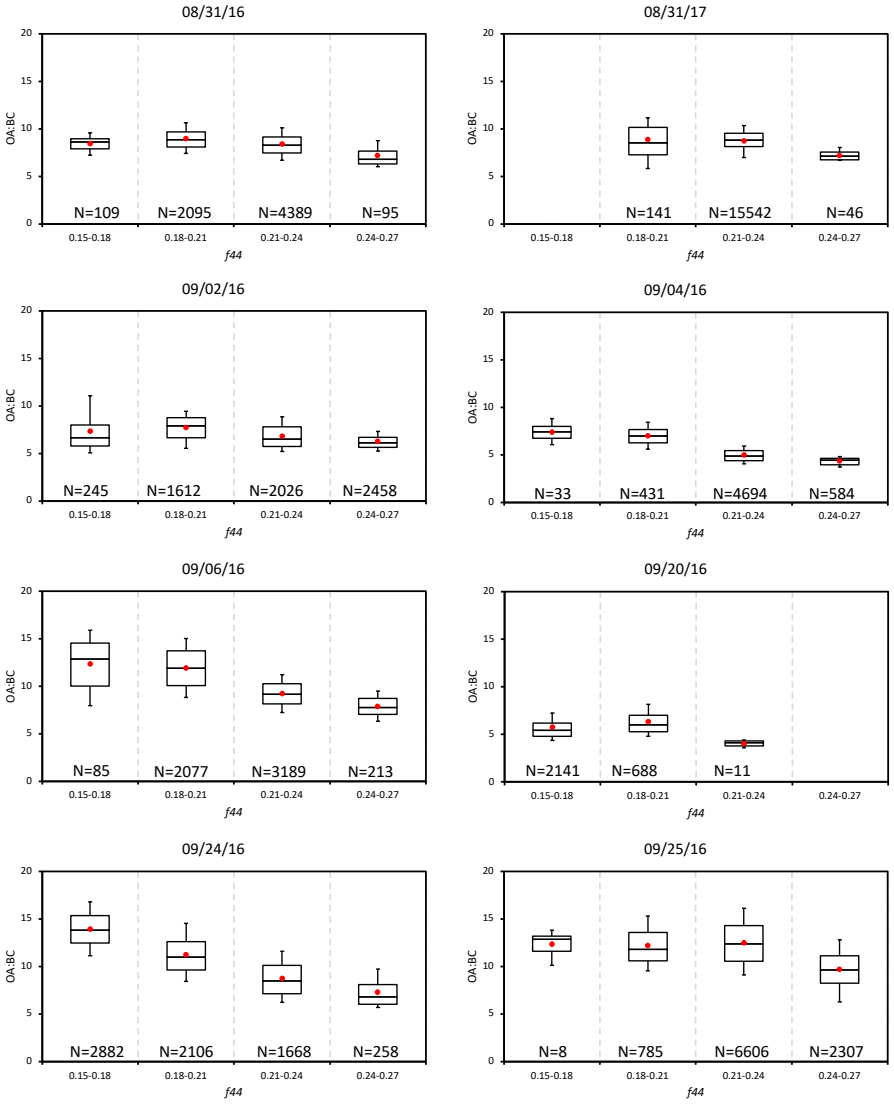

Figure S13. OA:BC mass ratios as a function of *f44* for the six flights. Whiskers represent the 10th and 90th percentiles, boxes illustrate the 75th and 25th percentiles with a line indicating the median and a red filled circle the mean. OA>10 μg m^{-3} only.